ASEAN
Journal of Scientific and Technological Reports
Online ISSN:2773-8752

Research article

The Batch Adsorption Process of Basic Dyes Using *Dialium Cochinchinensis* Seed Activated Carbon: Kinetics and Isotherms

Memoon Sattar[1] and Fareeda Hayeeye[2*]

[1] Faculty of Sports and Health Science, Thailand National Sports University, Yala Campus, 95000, Thailand
[2] Faculty of Science and Technology, Prince of Songkla University, Pattani Campus, 94000, Thailand
* Correspondence: fareedahayeeye@gmail.com

Citation:
Sattar, M.; Hayeeye, F. The batch adsorption process of basic dyes using *Dialium Cochinchinensis* seed activated carbon: kinetics and isotherms. *ASEAN J. Sci. Tech. Report*. **2026**, *29*(2), e260465. https://doi.org/10.55164/ajstr.v29i2.260465.

Article history:
Received: July 23, 2025
Revised: November 7, 2025
Accepted: December 3, 2025
Available online: January 21 2026

Abstract: The seeds of *Dialium cochinchinense*, an agricultural byproduct, were converted into an eco-friendly and cost-effective activated carbon (DSAC) for the adsorption of basic dyes, namely Rhodamine B (RB) and Crystal Violet (CV), from aqueous solutions. Batch adsorption experiments were performed to evaluate the effects of key parameters, including initial dye concentration, contact time, adsorbent dosage, and solution pH. The adsorption kinetics followed the pseudo-second-order model, indicating that chemisorption may play a role in the adsorption process. Equilibrium data were best fitted by the Langmuir isotherm model, with correlation coefficients (R^2) close to 1, suggesting monolayer adsorption. The maximum adsorption capacities (q_m) were 416.67 mg g^{-1} for RB and 526.32 mg g^{-1} for CV at 30 °C. These results demonstrate that DSAC is a sustainable, efficient, and economically viable adsorbent with strong potential for industrial wastewater treatment applications.

Keywords: ; *Dialium Cochinchinensis* seed; batch adsorption; basic dyes

1. Introduction

The paper, textile, and cosmetic industries extensively use synthetic dyes. Industrial effluents often contain various classes of dyes, such as anionic direct, reactive, nonionic disperse, and cationic dyes [1], many of which are toxic, resistant to degradation, and pose serious environmental concerns. Basic colors are often used on paper, wool, silk, acrylic fibers, and leather because of their high water solubility and vibrant color. Under dyeing conditions, dye molecules are also cationic dyes because the ammonium group in them carries a high positive charge [2, 3]. It has been estimated that nearly 100 tons of dyes and pigments are discharged into aquatic systems each week from industrial operations, contributing significantly to environmental contamination and posing risks to aquatic ecosystems. Additionally, the heavy metals contaminated in these dyes can be harmful, persistent, and nondegradable in the environment. These dyes pose a significant risk to aquatic life due to their potential mutagenic effects, as they greatly increase the chemical oxygen demand (COD) and biological oxygen demand (BOD) in water, indicating low oxygen levels [4]. Growing awareness of the environmental impact of organic loads has led to a steady rise in the demand for wastewater treatment over recent decades, driven by concerns about COD and BOD. The discharge of dye effluents has been identified as a cause of water pollution, requiring urgent action and remediation.

Industrial wastewater regulations mandate that BOD levels be less than 20 mg L^{-1} [5], but dye effluents can have very high BOD concentrations, sometimes reaching as high as 100,000 mg L^{-1}.

Several treatment methods have been employed to improve pollutant removal efficiency, including photocatalysis, coagulation, membrane separation, and adsorption [7, 11]. The adsorption process is widely used in wastewater treatment to eliminate pollutants. Adsorbents such as silica gel, zeolites, chitosan, natural fibers, magnetic nanocomposites, and activated carbon are commonly used in this approach [12–16]. Literature reviews have explored the synthesis of inexpensive adsorbents and the sustainability of dye adsorption using activated carbon derived from agricultural waste components [17]. *Dialium cochinchinense*, a commercially important plant grown in Thailand's Pattani province, was selected for the production of activated carbon (DSAC). DSAC is derived from agricultural waste that is abundantly available in the local area, as *Dialium cochinchinense* is commonly processed into seedless products for commercial use. Consequently, large quantities of seeds are discarded as waste. To add value to this byproduct, the seeds were utilized to produce granular activated carbon, which is easy to handle, cost-effective, and exhibits excellent adsorption performance. Rhodamine B (RB) and Crystal Violet (CV) were chosen as model adsorbates due to their toxicity. Basic dyes are visible in solution at concentrations below 1 ppm and have a high affinity for negatively charged adsorbent surfaces, facilitating the adsorption process [18]. Although the adsorption of basic dyes (RB and CV) by *Dialium cochinchinensis* seed activated carbon has been extensively studied, the adsorption capacities have often been found to be low [19–21]. Therefore, this study investigates the effectiveness of DSAC in removing RB and CV dyes.

2. Materials and Methods

2.1 Materials

Granular activated carbon derived from *Dialium cochinchinensis* seeds was prepared as follows: seeds were carbonized in a muffle furnace at 400°C for 3 h. The resulting char (DS) was then mixed with $ZnCl_2$ in a 1:1.5 ratio and activated at 450°C for an hour, representing the highest iodine number. The mixture was thoroughly washed with distilled water until the pH became neutral, followed by drying at 110 °C for 24 h. Additional details on the preparation can be found in Hayeeye et al. (2022) [22]. For pH regulation during the experiments, NaOH and HCl (Labscan, Ireland; Merck, Germany) were used. RB and CV dyes were purchased from Sigma-Aldrich. A primary stock solution (1,000 mg L^{-1}) of each dye was prepared by dissolving accurately weighed amounts in distilled water, and working solutions with concentrations ranging from 50 to 600 mg L^{-1} were obtained by appropriate dilution.

2.2 Methods

2.2.1 Characterization of DSAC

The specific surface areas of DSAC were determined using the nitrogen adsorption isotherm in the Brunauer-Emmett-Teller model, conducted with a Coulter SA 3100 analyzer at the Scientific Equipment Center, Prince of Songkla University. The pH drift method determined the point of zero charge (pH_{pzc}), where the surface of DSAC is neutral [23]. To do this, pH-adjusted 0.1 M NaCl solutions (pH 2 - 11) were prepared, and DSAC was added to 100 mL of each pH-adjusted NaCl solution. The flasks were sealed to prevent contact with air and left at ambient temperature for 24 hours. After stabilization, the final pH was recorded. The pH_{pzc} value of DSAC was determined by plotting the initial pH (pH_i) against the final pH (pH_f) and identifying the point where pH_i and pH_f were equal.

2.2.2 Batch adsorption experiments

The basic dyes (RB and CV) were selected for the adsorption process on DSAC. Batch adsorption experiments [24] were conducted to optimize various parameters, including initial dye concentration (50–600 mg L^{-1}), adsorbent dosage (0.1-0.6 g), contact time (0-20 h), and pH (2–9). Each parameter was studied individually while the other parameters were kept constant. In the experiments, 0.10 g of the adsorbent (DSAC) was added to 50 mL of the RB and CV solutions, and the mixtures were stirred in a shaking bath at 30 °C. The concentrations of RB and CV before and after the adsorption process were analyzed using the UV-Vis spectrophotometer, with absorbance measured at 554 and 591 nm for RB and CV, respectively. The RB and

CV residual concentrations were calculated based on previously determined calibration curves. The residual RB and CV concentrations were calculated based on the previously determined calibration curve. The percentage removal and the adsorption capacity, q_e (mg g^{-1}) of RB and CV on DSAC were then determined according to equations (1) and (2) [24] as follows:

$$\%RE = \frac{C_0 - C_e}{C_0} \times 100 \quad (1)$$

$$q_e = \frac{V(C_0 - C_e)}{W} \quad (2)$$

where W is the dosage of adsorbent (g), V is the volume of the basic dye solutions (L), C_0 and C_e are the initial and equilibrium liquid-phase concentrations of RB and CV (mg L^{-1}), respectively. Kinetic experiments were conducted with initial basic dye concentrations of 50 and 100 mg L^{-1} for RB and CV, maintaining a constant initial pH. The DSAC adsorbent was introduced into 50 mL of the basic dye solutions, which were then continuously shaken. At pre-determined sampling times, 1 mL solution samples were withdrawn using a syringe and analyzed for RB and CV residuals using UV-vis spectrophotometry. The experiments were repeated in triplicate to ensure the reliability of the results. The adsorption experiments were performed to investigate the different effects using 50 mL of 100 mg L^{-1} RB and CV solutions at their natural pH values: pH 4.0 for RB and pH 5.0 for CV. The equilibrium data were further evaluated using the pseudo-first-order and pseudo-second-order adsorption kinetic models as well as various adsorption isotherms, namely the Langmuir, Freundlich, Temkin, and Dubinin–Radushkevich models. [22].

2.2.3 Kinetic models for the adsorption process

The kinetic adsorption models describe the adsorption rate over time, offering insight into the underlying adsorption mechanism. The most commonly applied models are the pseudo-first-order (Lagergren's model) [25] and pseudo-second-order (Ho and McKay's model) [26]. These models are represented by equations (3) and (5), respectively, and can be expressed in their linear forms as equations (4) and (6).

$$\frac{dq_t}{dt} = k_1(q_e - q_t) \quad (3)$$

$$\ln(q_e - q_t) = \ln q_e - k_1 t \quad (4)$$

$$\frac{dq_t}{dt} = k_2(q_e - q_t)^2 \quad (5)$$

$$\frac{t}{q_t} = \frac{1}{k_2 q_e^{\,2}} + \frac{1}{q_e} t \quad (6)$$

Where q_e and q_t were the amount of dye adsorbed (mg g^{-1}) at equilibrium and at any time. k_1 and k_2 were the pseudo-first-order rate constant (min^{-1}) and the pseudo-second-order-rate constant (g mg^{-1} min^{-1}), respectively.

2.2.4 Isotherm models for the adsorption process

Several isotherm models, including the Langmuir, Freundlich, Temkin, and Dubinin–Radushkevich isotherms, were tested to fit the adsorption equilibrium data. These isotherms were represented by the following linear form in equations (7) to (10) [27 - 30]

$$\frac{C_e}{q_e} = \frac{1}{q_m b} + \frac{C_e}{q_m} \tag{7}$$

$$\log q_e = \log K_F + \frac{1}{n}\log C_e \tag{8}$$

$$q_e = B\ln A_t + B\ln C_e \;; B = \frac{RT}{b} \tag{9}$$

$$\ln q_e = \ln q_s - K_d \varepsilon^2 \;; \varepsilon = RT\ln\left(1+\frac{1}{C_e}\right) \tag{10}$$

Where C_e is the equilibrium concentration (mg L^{-1}), q_e is the amount adsorbed at equilibrium (mg g^{-1}), respectively. The parameters of q_m and b are Langmuir constants representing the maximum adsorption capacity (mg g^{-1}) and the adsorption equilibrium constant (L mg^{-1}), respectively. The values of K_F and n are Freundlich constants, indicating the adsorption capacity (L g^{-1}) and the adsorption intensity, respectively. A_t is the Temkin isotherm equilibrium binding constant (L g^{-1}), R is a universal gas constant (8.314 J $mol^{-1}K^{-1}$), T signifies temperature at 298K, and B is a constant related to the heat of sorption (J mol^{-1}). The q_s is a theoretical isotherm saturation capacity (mg g^{-1}), K_d is the Dubinin–Radushkevich isotherm constant (mol^2 kJ^{-2}), and ε is the Dubinin–Radushkevich isotherm constant.

3. Results and Discussion

3.1 Characterization of DSAC

The specific surface area of DSAC was evaluated based on the Brunauer–Emmett–Teller (BET) model [31]. As shown in Figure 1, the N_2 adsorption isotherms were interpreted according to the IUPAC classification, which distinguishes six types of adsorption isotherms [32]. Type I adsorption isotherms are typically used for tiny pores or microporous adsorbents, where the rate of adsorbate adsorption depends on available micropore volume rather than total interior surface area. Types II, III, and VI were observed in non-porous or macroporous materials. Type III and Type V isotherms indicate stronger adsorbate-adsorbate interactions compared to adsorbate-adsorbent interactions. Types IV and V were identified for mesoporous materials. The hysteresis loop type H4 suggests the presence of mesoporous particles [33-35]. DSAC predominantly exhibits mesoporous characteristics, classifying it as a Type IV adsorbent. The activated carbon prepared with $ZnCl_2$ is mainly microporous but contains a significant mesopore component, which increases with the $ZnCl_2$-to-precursor impregnation ratio [36, 37].

The BET surface area of DSAC was calculated (Table 1) and may significantly influence its adsorption efficiency. Notably, DSAC showed a substantial BET-specific surface area alongside increased mesopore volume. The physical properties of the raw materials likely influenced the porosity characteristics of the final activated carbon products. Additionally, the BET surface area values of DSAC are considerably higher than those of modified granular composite adsorbents such as chitosan-bentonite-zirconium chloride (Cs- Bn- Zr), S/modified bentonite (GOMBt), granular bentonite (GBt), ZnO-chitosan beads (CZB), chitosan beads (CB), and chitosan beads coated with ZnO (ZCB), as shown in Table 1 [38-40]. The pH_{pzc} graphs were plotted between the pH_f and the pH_i for DSAC, as shown in Figure 2. The pH_{pzc} value of DSAC was found to be 3.5, indicating that DSAC carries a positive charge. This positive charge causes electrostatic repulsion with the positive charges of basic dyes [41]. Consequently, DSAC is attracted to negatively charged species, enabling it to adsorb RB and CV solutions at pH 4 and pH 5, respectively. Moreover, the morphology of the DSAC bead shows numerous pores on the surface.

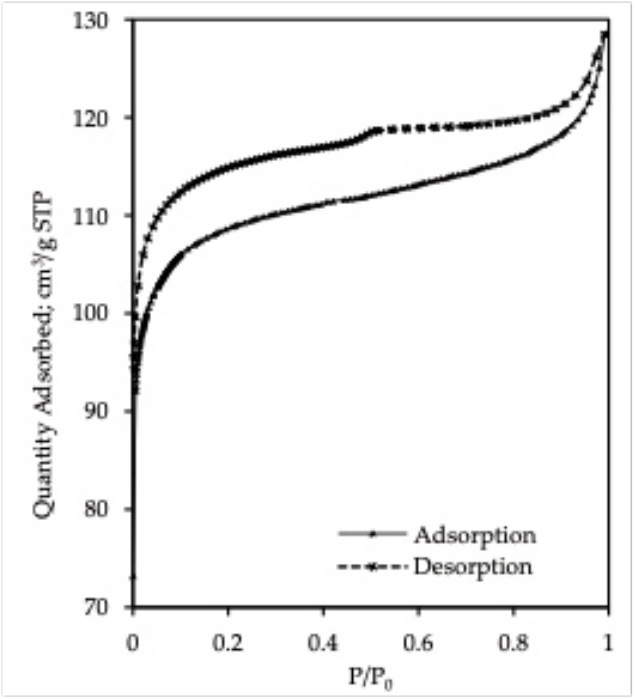

Figure 1. N_2 adsorption isotherm of DSAC: Note the hysteresis in types IV and V [32].

Table 1. BET surface area of DSAC compared with the granular adsorbents

Sample	BET Specific Surface area ($m^2\ g^{-1}$)	Micropore volume ($cm^3\ g^{-1}$)	Average pore size (nm)	Ref.
DSAC	290.19	0.109	4.96	This study
Cs-Bn-Zr	63.80	0.095	3.57	[38]
GOMBt	36.50	0.097	3.83	[39]
GBt	35.65	0.076	3.84	
CB	12.46	0.013	3.89	
CZB	13.11	0.016	3.74	[40]
ZCB	13.54	0.018	3.63	

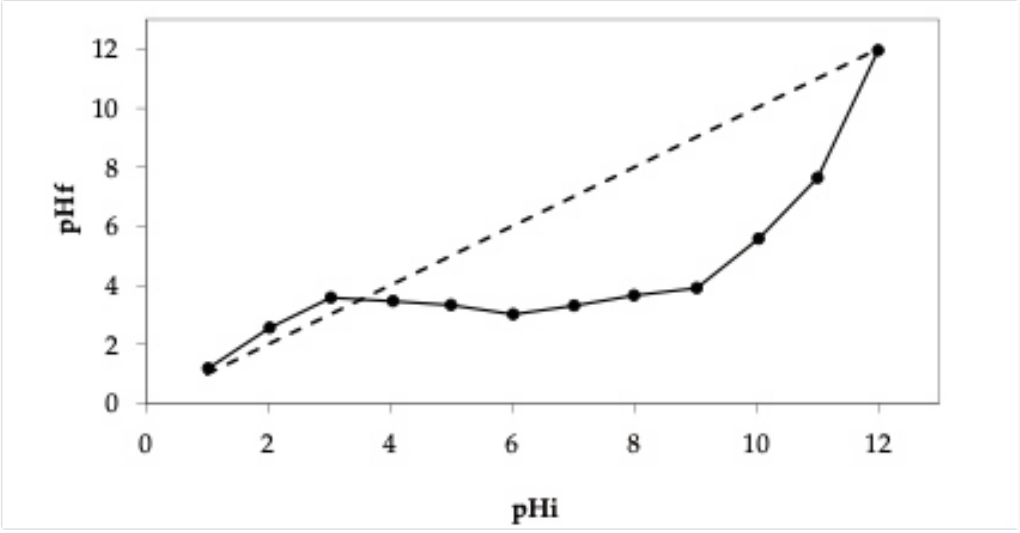

Figure 2. The pH_{pzc} of DSAC

3.2 Effects of various parameters in adsorption studies

Figure 3 illustrates the effect of contact time and initial concentrations of RB and CV on DSAC. The results reveal equilibrium times of approximately 12 hours for RB and 7 hours for CV solutions. Moreover, the amount adsorbed at equilibrium (q_e) rises with increasing initial concentrations of RB and CV solutions, suggesting potential interactions between the basic dye solutions and the adsorbents [42]. The adsorbent dosage from 0.10 - 0.60 g was used to study the effect of DCS-AC dosage for removing 100 mg L^{-1} of RB and CV solutions at 30 °C as shown in Figure 4. At equilibrium, the percentage removal of RB and CV solutions increased with increasing DSAC dosage. However, the amount of adsorbed (q_e) decreased with increasing the DSAC dosage. The result indicated that an increase in adsorbent dosage increases the surface area and availability of adsorption sites [43]. There are the highest amounts adsorbed at equilibrium, 56.97 mg g^{-1} (RB) and 71.62 mg g^{-1} (CV), on the optimal DSAC dosages, with the maximum amount of adsorbed values being 0.10 g, which is appropriate to use in this study.

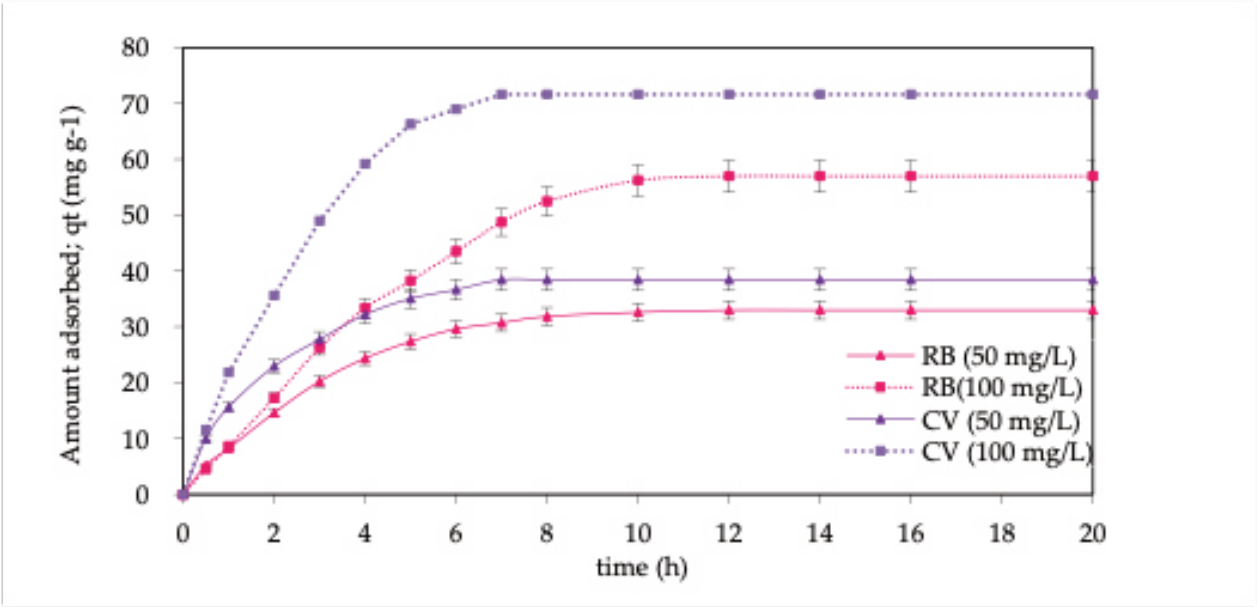

Figure 3. The effect of contact time and initial concentration of RB (pH 4.0) and CV (pH 5.0) on DSAC at 30°C (50 and 100 mg/L of basic dye solutions, 0.10 g of DSAC)

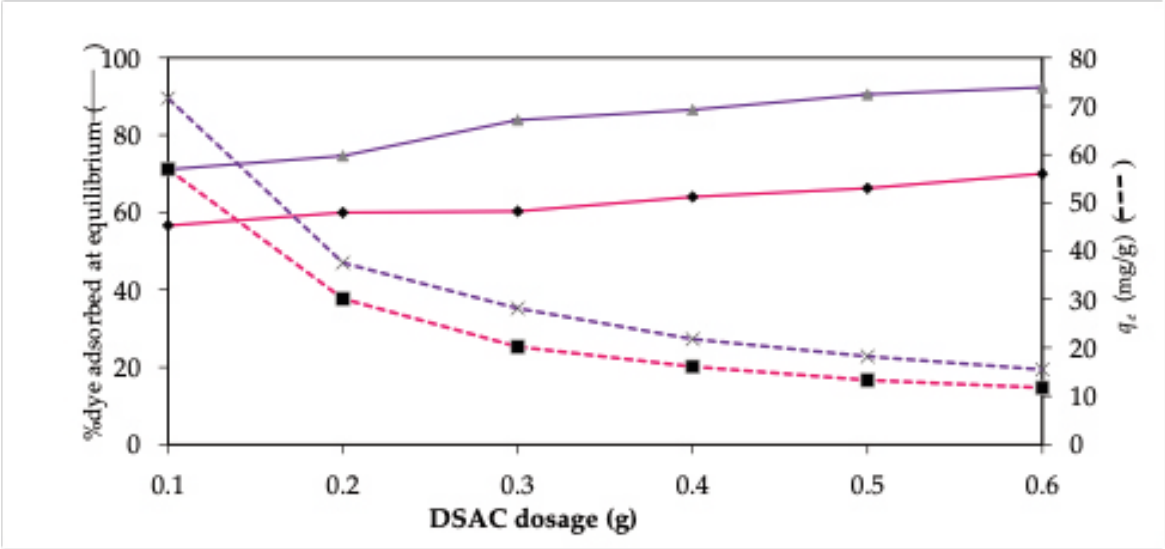

Figure 4. The effect of DSAC dosage on the adsorption of 100 mg L^{-1} of RB (pH 4) and CV (pH 5)

The pH factor is critical in adsorption, particularly for dye adsorption. As illustrated in Figure 5, the adsorption of RB and CV on DSAC increases slightly as the pH rises above 2. At lower pH levels, protonation causes H^+ ions to compete with RB and CV molecules for adsorption sites on the DSAC surface. Below the pHpzc (3.5), the DSAC surface is positively charged, whereas above pHpzc it becomes negatively charged. The pH increases, the electrical repulsion weakens, enabling more RB and CV molecules to adsorb onto the activated carbon. Conversely, at pH levels above 7, OH^- ions compete with RB and CV molecules for adsorption sites, and due to their smaller size, OH^- ions may migrate more quickly to the activated carbon surface, the generation of hydrogen bonds between the carboxylic groups of RB or CV and the beads potentially impact RB and CV of adsorption efficiency [44, 45].

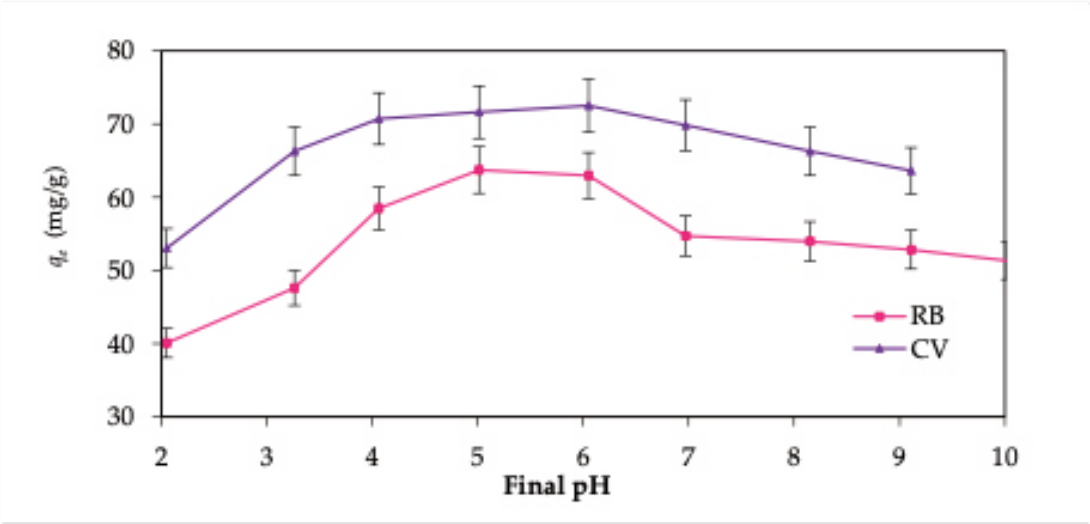

Figure 5. The effect of pH of RB and CV adsorption on DSAC at 30°C (100 mg/L of basic dye solutions, 0.10 g of DSAC)

3.3 Kinetic models for the adsorption process

The Kinetic models were employed to understand the adsorption mechanisms behind the interactions between adsorbate and adsorbent [25, 26]. The experimental results were fitted using pseudo-first-order and pseudo-second-order kinetic models. Linear plots of $ln(q_e - q_t)$ versus t for the pseudo-first-order model and t/q_t versus t for the pseudo-second-order model are shown in Figure 6. The values of k_1 and k_2 were determined from the slopes of the straight lines. Various kinetic parameters, including the correlation coefficient R^2, are listed in Table 2. The results suggest that the adsorption kinetics of RB and CV onto DSAC are most accurately represented by the pseudo-second-order model, as evidenced by the R^2 values being closest to unity. The adsorption process on porous materials proceeds through three stages: adsorption on the external surface, a gradual adsorption phase, and adsorption within the internal surface, ultimately reaching equilibrium. [46].

Table 2. Parameters of kinetic models for RB and CV solutions on DSAC

Kinetic models	Parameter	Value			
		RB (mg L^{-1})		CV (mg L^{-1})	
		50	100	50	100
Pseudo–first order	q_e (mg g^{-1})	4.91	6.41	4.96	7.31
	k_1 (× 10^{-3})	3.0	2.2	3.6	4.1
	R^2	0.97	0.96	0.98	0.95
Pseudo – second order	q_e (mg g^{-1})	52.36	136.99	49.75	131.58
	k_2 (× 10^{-5})	6.56	0.98	1.53	0.25
	R^2	0.98	0.97	0.99	0.98

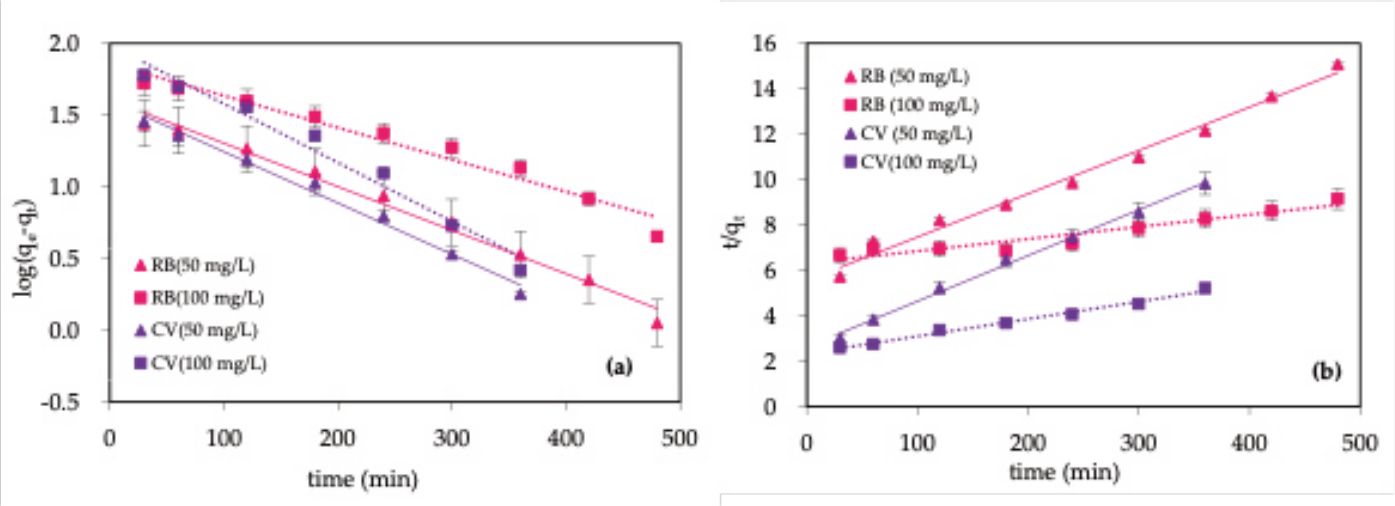

Figure 6. The kinetic adsorption models: (a) pseudo-first-order and (b) pseudo-second-order models, for RB and CV (50 and 100 mg L^{-1}) adsorption on DSAC, at 30°C and pH 5 (0.10 g of DSAC)

3.4 Isotherm models for the adsorption process

Mathematical models for representing adsorption isotherms have been developed. The Langmuir model in equations (7) suggests monolayer adsorption on a homogeneous surface of the adsorbent at the interface between the solid and liquid phases, and it also estimates the maximum adsorption capacity of the process [27]. Furthermore, the Freundlich isotherm in equations (8) is commonly used to describe the exponential adsorption of target compounds on heterogeneous surfaces. K_f indicates the strength of adsorption, with lower values indicating stronger adsorption. Another constant, $1/n$, indicates the adsorption intensity, and favorable adsorption is typically observed when the n value is between 1 and 10 [28, 48]. The Temkin isotherm detailed in equation (9) includes a factor that explicitly accounts for adsorbent–adsorbate interactions and assumes that the heat of adsorption of all molecules in the layer decreases linearly rather than logarithmically with coverage. This derivation features a uniform distribution of maximum binding energies. The Dubinin–Radushkevich isotherm (equation 10) is generally applied to describe the adsorption mechanism with a Gaussian energy distribution on a heterogeneous surface. This approach is often used to distinguish between physical and chemical adsorption, with the mean free energy E per molecule of adsorbate calculated using equation (11) [30, 47].

$$E = \frac{1}{\sqrt{2K_d}} \tag{11}$$

The mean adsorption energy (E) can describe adsorption properties. When the value of E was less than 8 kJ mol^{-1}, it followed physical adsorption, but when the value of E ranged from 8 to 16, it followed chemical adsorption [30, 48]. The Langmuir, Freundlich, Temkin, and Dubinin–Radushkevich isotherms were shown in Figure 7. All the parameters derived from these four isotherms, including the correlation coefficients, are summarized in Table 3. The parameters were calculated based on the slope and intercept of the respective isotherm equations. The results indicated that the adsorption process of RB and CV solutions on the DSAC corresponded more closely with the Langmuir isotherm model than with the Freundlich, Temkin, and Dubinin–Radushkevich models, as evidenced by a higher correlation coefficient (R^2). Therefore, the Langmuir equation was chosen as the best match for the adsorption isotherms. Moreover, this further means that the adsorption suggested monolayer adsorption on a homogeneous surface, according to Langmuir's theory. The DSAC surface is relatively homogenous regarding functional groups with significant interaction with RB and CV molecules [22, 49]. The Langmuir equation determined the maximum adsorption capacities (q_m) on DSAC to be 416.67 mg g^{-1} for RB and 526.32 mg g^{-1} for CV solutions. Table 4 provides the maximum uptake capacities (q_m) for RB and CV solutions compared with some reported activated carbons synthesized from different

sources. The results indicate that the qm values for RB and CV removal on DSAC were higher than those achieved with other biomass-derived activated carbons. This suggests that the DSAC adsorbent developed in the current study demonstrates superior performance. Notably, DSAC offers significant advantages over other carbon-based adsorbents; Therefore, DSAC is an effective adsorbent material for treating wastewater.

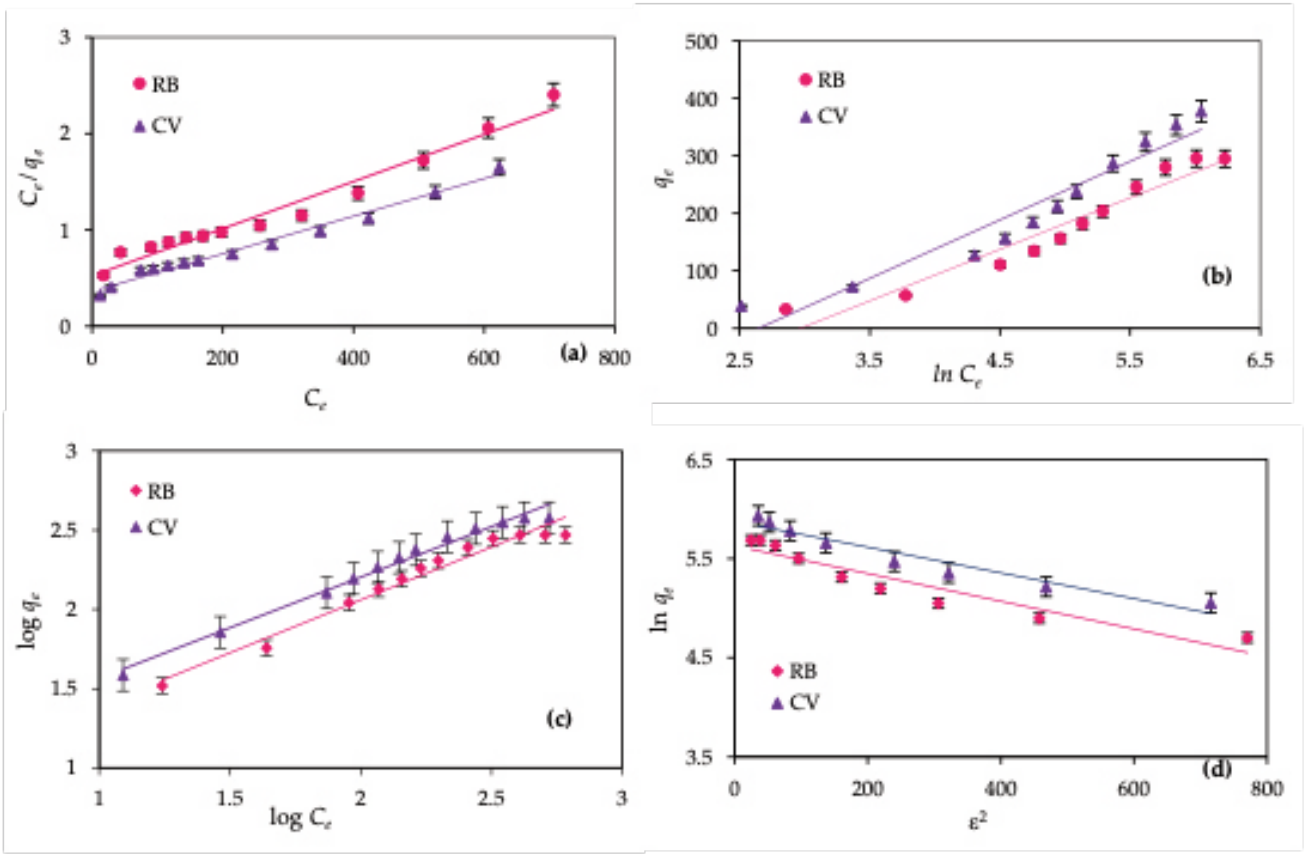

Figure 7. The (a) Langmuir, (b) Freundlich, (c) Temkin, and (d) Dubinin–Radushkevich isotherms of RB (pH 4.0) and CV (pH 5.0) solutions on DSAC (basic dye concentration 50–600 mg L^{-1}, 0.10 g of DSAC)

Table 3 Parameter of Langmuir, Freundlich, Temkin, and Dubinin–Radushkevich for RB and CV on DSAC

No.	Adsorbents	*pH*	q_m (mg g^{-1})	*Ref.*
	RB			
1.	Polysulfone - AC	4.0	25.71	[20]
2.	White sugar AC	4.0	123.46	[45]
3.	Magnetic AC	4.0	135.01	[50]
4.	Cassava peel	4.0	265.36	[51]
5.	DSAC	4.0	416.67	This study
	CV			
6.	Date palm leaves AC	5.0	37.58	[21]
7.	Korean cabbage waste	5.0	195.60	[52]
8.	NaOH-activated Aerva javanica leaf	5.0	315.20	[53]
9.	Water hyacinth plants AC	5.0	322.58	[54]
10.	DSAC	5.0	526.32	This study

Table 4. The maximum adsorption capacities of RB and CV compared with prior literature at 25 °C

Isotherms	Parameters	Value	
		RB	CV
Langmuir	q_m (mg g^{-1})	416.67	526.32
	b (L mg^{-1})	0.004	0.005
	R^2	0.97	0.98
Freundlich	K_F (L g^{-1})	4.65	4.35
	n	1.38	1.08
	R^2	0.96	0.97
Temkin	A_T (L g^{-1})	0.05	0.07
	B (J mol^{-1})	89.55	101.63
	R^2	0.93	0.92
Dubinin–Radushkevich	K_d (mol^2 kJ^{-2}) ×10^{-3}	1.41	1.30
	q_s (mg g^{-1})	278.66	354.25
	E (kJ mol^{-1})	0.18	0.19
	R^2	0.89	0.93

4. Conclusions

Dialium cochinchinense seed–based activated carbon (DSAC) was successfully prepared using $ZnCl_2$ activation and demonstrated high efficiency in removing Rhodamine B (RB) and Crystal Violet (CV) from aqueous solutions. The adsorption followed the pseudo-second-order kinetic model and fitted well with the Langmuir isotherm, showing maximum adsorption capacities of 416.67 mg g^{-1} for RB and 526.32 mg g^{-1} for CV at 30 °C. Removal efficiencies ranged between 80% and 90%, confirming the strong adsorption performance of DSAC. These findings highlight DSAC as a cost-effective, sustainable, and environmentally friendly adsorbent derived from agricultural waste. With its simple preparation, high adsorption capacity, and reusability potential, DSAC shows great promise for practical application in industrial wastewater treatment systems.

5. Acknowledgements

The authors wish to extend their sincere thanks to the Department of Science, Faculty of Science and Technology, Prince of Songkla University, Pattani Campus, Thailand, and the Thailand National Sport Science University, Yala Campus, for their invaluable support.

Author Contributions: Conceptualization, experimental design, Sattar, M, conducting experiments and data acquisition, Hayeeye, F., data analysis, writing and editing, Hayeeye, F., and Sattar, M. All authors have read and approved the published version of the manuscript.

Funding: None.

Conflicts of Interest: The authors declare no conflict of interest.

References

[1] Benkhaya, S.; El Harfi, S.; El Harfi, A. Classifications, Properties, and Applications of Textile Dyes: A Review. *Appl. J. Environ. Eng. Sci.* **2017**, *3*(3), 311–320.

[2] Qada, E. N.; Allen, S. J.; Walker, G. M. Adsorption of Basic Dyes from Aqueous Solution onto Activated Carbons. *Chem. Eng. J.* **2008**, *135*(3), 174–184. https://doi.org/10.1016/j.cej.2007.02.023

[3] Massoud, K.; Motaba, S.; Sahar, M. Removal of Dyes from the Environment by Adsorption Process. *Chem. Mater. Eng.* **2018**, *6*(2), 31–35. https://doi.org/10.13189/cme.2018.060201

[4] Sasan, F.; Gholian, J.; Konečný, J. J.; Baloch, A.; Kordestani, H. K. Sustainable and Optimized Values for Municipal Wastewater: Removal of BOD and COD Using Granular Activated Carbon and Genetic Algorithm-Based Simulation. *J. Clean. Prod.* **2023**, *417*, 137932. https://doi.org/10.1016/j.jclepro.2023.137932

[5] Sarakarnkosol, W. Pollution and Risk of Wastewater from Textile Dyeing Process. *Environ. J.* **2017**, *21*(1), 7–14 (in Thai).

[6] Surafel, M. B.; Venkatesa, P.; Tsegaye, S.; Abraham, G. Sugarcane Bagasse-Based Activated Carbon Preparation and Its Adsorption Efficacy for Removal of BOD and COD from Textile Effluents. *Bioresour. Technol. Rep.* **2021**, *14*, 100664. https://doi.org/10.1016/j.biteb.2021.100664

[7] Ibrahim, E. S.; Laszlo, E.; Kim, J.-H.; Kim, H. S. Adsorption and Photocatalytic Degradation of Methylene Blue over Hydrogen-Titanate Nanofibres. *Water Res.* **2013**, *47*(12), 4115–4125. https://doi.org/10.1016/j.watres.2012.12.045

[8] Vijayaraghavan, G.; Shanthakumar, S. Effective Removal of Reactive Magenta Dye in Textile Effluent by Coagulation Using Algal Alginate. *Desalin. Water Treat.* **2018**, *121*, 22–27. https://doi.org/10.5004/dwt.2018.22190

[9] Wang, Y.; Liu, C.; Ma, M.; Li, P.; Li, X.; Yu, Y. Fabrication and Evaluation of GO/TiO_2-Based Molecularly Imprinted Nanocomposite Membranes. *Sep. Purif. Technol.* **2019**, *212*, 245–254. https://doi.org/10.1016/j.seppur.2018.11.042

[10] Chakraborty, S.; Chowdhury, S.; Das Saha, P. Adsorption of Crystal Violet from Aqueous Solution onto NaOH-Modified Rice Husk. *Carbohydr. Polym.* **2011**, *86*(4), 1533–1541. https://doi.org/10.1016/j.carbpol.2011.06.058

[11] Hayeeye, F.; Sattar, M.; Tekasakul, S.; Sirichote, O. Adsorption of Rhodamine B on Activated Carbon from Rubber Fruit Pericarp. *Songklanakarin J. Sci. Technol.* **2014**, *36*(2), 177–187.

[12] Gaikwad, R. W.; Misal, S. A. Sorption Studies of Methylene Blue on Silica Gel. *Int. J. Chem. Eng. Appl.* **2010**, *1*(4), 342–345. https://doi.org/10.7763/IJCEA.2010.V1.59

[13] Imessaouden, A.; Cheikh, S.; Hadadi, A.; Hamri, N.; Bollinger, J.-C.; Amrane, A.; Tahraoui, H.; Manseri, A.; Mouni, L. Adsorption Performance of Zeolite for Congo Red Removal. *Separations* **2023**, *10* (1), 57. https://doi.org/10.3390/separations10010057

[14] Sarkar, T. K.; Chakraborty, N.; Basu, S.; Ghosh, A.; Inoue, H.; Fukumori, Y. Adsorption of Methyl Orange onto Chitosan. *J. Water Resour. Prot.* **2010**, *2*, 898–906. https://doi.org/10.4236/jwarp.2010.210107

[15] Basha, N. A.; Rathinavel, T.; Sridharan, H. Activated Carbon from Coconut Shell: Synthesis and Applications. *Appl. Sci. Eng. Prog.* **2023**, *16*(2), 6152. https://doi.org/10.14416/j.asep.2022.07.001

[16] Esvandi, Z.; Foroutan, R.; Peighambardoust, S. J.; Akbari, A.; Ramavandi, B. Uptake of Anionic and Cationic Dyes from Water Using Natural Clay and Clay/Starch/$MnFe_2O_4$ Magnetic Nanocomposite. *Surf. Interfaces* **2020**, *21*, 100754. https://doi.org/10.1016/j.surfin.2020.100754

[17] Bharathi, K. S.; Ramesh, S. T. Removal of Dyes Using Agricultural Waste as Low-Cost Adsorbents: A Review. *Appl. Water Sci.* **2013**, *3*, 773–790. https://doi.org/10.1007/s13201-013-0117-y

[18] Emad, N.; Qada, E. N.; Allen, S. J.; Walker, G. M. Adsorption of Basic Dyes from Aqueous Solution onto Activated Carbons. *Chem. Eng. J.* **2008**, *135*(3), 174–184. https://doi.org/10.1016/j.cej.2007.02.023

[19] Laktif, T.; Lakhmiri, R.; Albourine, A. *Salsola tetragona* as a New Low-Cost Adsorbent for Water Treatment: Highly Effective Adsorption of Crystal Violet. *Int. J. Phytoremediation* **2024**, *26*, 1691–1700. https://doi.org/10.1080/15226514.2024.2349703

[20] Sattar, M.; Hayeeye, F.; Chinpa, W.; Sirichote, O. Preparation and Characterization of Polysulfone/Activated Carbon Composite Beads. *Appl. Mech. Mater.* **2014**, *625*, 106–109. https://doi.org/10.4028/www.scientific.net/AMM.625.106

[21] Ghazali, A.; Shirani, M.; Semnani, A.; Zare-Shahabadi, V.; Nekoeini, M. Optimization of Crystal Violet Adsorption onto Date Palm Leaves as a Potent Biosorbent Using Response Surface Methodology and Ant Colony Optimization. *J. Environ. Chem. Eng.* **2018**, *6*, 3942–3950. https://doi.org/10.1016/j.jece.2018.05.043

[22] Hayeeye, F.; Benhawan, A.; Sattar, M. Adsorption Efficiency of Batik Dye by Modified *Dialium cochinchinense* Activated Carbon Beads: Kinetics and Thermodynamics. *Desalin. Water Treat.* **2022**, *269*, 200–211. https://doi.org/10.5004/dwt.2022.28751

[23] Jia, Y. F.; Xiao, B.; Thomas, K. M. Adsorption of Metal Ions on Nitrogen Surface Functional Groups in Activated Carbons. *Langmuir* **2002**, *18*, 470–478. https://doi.org/10.1021/la011161z

[24] Hayeeye, F.; Sattar, M.; Chinpa, W.; Sirichote, O. Kinetics and Thermodynamics of Rhodamine B Adsorption by Gelatin/Activated Carbon Composite Beads. *Colloids Surf., A* **2017**, *513*, 259–266. https://doi.org/10.1016/j.colsurfa.2016.10.052

[25] Lagergren, S. Zur Theorie der Sogenannten Adsorption Gelöster Stoffe. *Kungl. Svenska Vetenskapsakad. Handl.* **1898**, *24*, 1–39.

[26] Ho, Y. S.; McKay, G. Pseudo-Second-Order Model for Sorption Processes. *Process Biochem.* **1999**, *34*, 451–465. https://doi.org/10.1016/S0032-9592(98)00112-5

[27] Langmuir, I. Adsorption of Gases on Plane Surfaces of Glass, Mica, and Platinum. *J. Am. Chem. Soc.* **1918**, *40*, 1361–1403. https://doi.org/10.1021/ja02242a004

[28] Freundlich, H. Über die Adsorption in Lösungen. *Z. Phys. Chem.* **1907**, *57*, 385–470. https://doi.org/10.1007/BF01813604

[29] Al-Shehri, A.; Almudaifer, E. A.; Alorabi, A. Q.; Alanazi, H. S.; Alkorbi, A. S.; Alharthi, F. A. Effective Adsorption of Crystal Violet from Aqueous Solutions: Equilibrium, Mechanism Studies, and Modeling Analysis. *Environ. Pollut. Bioavailability* **2021**, *33*(1), 214–226. https://doi.org/10.1080/26395940.2021.1960199

[30] Dubinin, M. M. The Potential Theory of Adsorption of Gases and Vapors for Adsorbents with an Energetically Nonuniform Surface. *Chem. Rev.* **1960**, *60*, 235–266. https://doi.org/10.1021/cr60204a006

[31] Brunauer, S.; Skalny, J.; Bodor, E. E. Adsorption on Nonporous Solids. *J. Colloid Interface Sci.* **1969**, *30*(4), 546–552. https://doi.org/10.1016/0021-9797(69)90423-8

[32] Zeid, A.; Othman, A. Fundamental Aspects of Silicate Mesoporous Materials: A Review. *Materials* **2015**, *8*(12), 2874–2902. https://doi.org/10.3390/ma5122874

[33] Broekhoff, J. C. Mesopore Determination from Nitrogen Sorption Isotherms: Fundamentals, Scope, and Limitations. *Stud. Surf. Sci. Catal.* **1979**, *36*, 63–84.

[34] Sing, K. S. W.; Everett, D. H.; Haul, R. A. W.; Moscou, L.; Pierotti, R. A.; Rouquerol, J.; Siemieniewska, T. Reporting Physisorption Data for Gas/Solid Systems. *Pure Appl. Chem.* **1985**, *57*, 603–619. https://doi.org/10.1351/pac198557040603

[35] Abebe, B.; Murthy, H. A.; Amare, E. Summary on Adsorption and Photocatalysis for Pollutant Remediation: A Mini-Review. *J. Encapsulation Adsorpt. Sci.* **2018**, *8*, 225–255. https://doi.org/10.4236/jeas.2018.84012

[36] McEnaney, B.; Schüth, F.; Sing, K. S. W.; Weitkamp, J. *Handbook of Porous Solids*; Wiley-VCH: Weinheim, Germany, **2002**; Vol. 1.

[37] Azargohar, R. *Production of Activated Carbon and Its Catalytic Application for Oxidation of Hydrogen Sulphide*; Ph.D. Thesis, University of Saskatchewan, **2009**.

[38] Jamka, Z.; Mohammed, W. Feasibility of Modified Chitosan Beads for Nitrate Adsorption from Aqueous Solution. *J. Ecol. Eng.* **2023**, *24*(2), 265–278. https://doi.org/10.12911/22998993/156886

[39] Zhou, J.; Sun, Q. Sodium Alginate/Modified Bentonite Composite Beads for Adsorptive Removal of Norfloxacin. *Polymers* **2022**, *14*(19), 3984–4001. https://doi.org/10.3390/polym14193984

[40] Ngamsurach, P.; Namwongsa, N.; Praipipat, P. Synthesis of ZnO-Modified Chitosan Materials for Pb(II) Removal. *Sci. Rep.* **2022**, *12*, 17184. https://doi.org/10.1038/s41598-022-22182-4

[41] Hayeeye, F.; Sattar, M. Removal of Crystal Violet by Activated Carbon from Rubber Fruit Pericarp and Bagasse. *Desalin. Water Treat.* **2020**, *202*, 420–434. https://doi.org/10.5004/dwt.2020.26152

[42] Asaad, H. F.; Elhadidly, H. Production of Activated Carbons from Waste Carpets for Methylene Blue Adsorption. *J. Environ. Chem. Eng.* **2017**, *5*, 955–963. https://doi.org/10.1016/j.jece.2017.01.003

[43] Ghaedi, M.; Ansari, A.; Habibi, M. H.; Asghari, A. R. Removal of Malachite Green Using ZnO Nanoparticles Loaded on Activated Carbon. *J. Ind. Eng. Chem.* **2014**, *20*, 17–28. https://doi.org/10.1016/j.jiec.2013.04.031

[44] Porkodi, K.; Vasanth, K. K. Modeling and Simulation of Dye Sorption onto Jute Fiber Carbon. *J. Hazard. Mater.* **2007**, *143*, 311–327. https://doi.org/10.1016/j.jhazmat.2006.09.029

[45] Xiao, W.; Garba, Z. N.; Sun, S.; Lawan, I.; Wang, L.; Lin, M.; Yuan, Z. Activated Carbon from White Sugar for Rhodamine B Adsorption. *J. Clean. Prod.* **2020**, *253*, 119989. https://doi.org/10.1016/j.jclepro.2020.119989

[46] Ghaedi, M.; Ghaedi, A. M.; Negintaji, E.; Ansari, A.; Vafaei, A.; Rajabi, M. Random Forest Model for Bromophenol Blue Removal Using Activated Carbon. *J. Ind. Eng. Chem.* **2014**, *20*, 1793–1803. https://doi.org/10.1016/j.jiec.2013.08.033

[47] Dada, A. O.; Olalekan, A. P.; Olatunya, A. M. Langmuir, Freundlich, Temkin, and Dubinin–Radushkevich Isotherm Studies of Zn^{2+} Adsorption. *J. Appl. Chem.* **2012**, *3*(1), 38–45. https://doi.org/10.9790/5736-0313845

[48] Azad, M. S.; Mohd, S. H.; Shahinuzzaman, M.; Azhari, S. Removal of Copper from Aqueous Solution Using Rice Husk Activated Carbon. *Sci. Technol. Asia* **2022**, *27*(3), 69–84.

[49] Arabzadeh, S.; Ghaedi, M.; Ansari, A.; Taghizadeh, F.; Rajabi, M. Removal of Methylene Blue Using NiO and Pd Nanoparticle-Loaded Activated Carbon. *Hum. Exp. Toxicol.* **2015**, *34*, 153–169. https://doi.org/10.1177/0960327114532383

[50] Boulder, B.; Rida, K. Adsorption of Rhodamine B, Methyl Orange, and Phenol by Magnetic Activated Carbon. *Mater. Sci. Eng. B* **2024**, *307*, 117502. https://doi.org/10.1016/j.mseb.2024.117502

[51] Belcaid, A.; Beakou, B. H.; Bouhsina, S.; Anouar, A. Adsorptive Removal of Dyes by Cassava Peel Biochar. *Biofuels, Bioprod. Biorefin.* **2024**, *14*, 7783–7806. https://doi.org/10.1007/s13399-022-02928-w

[52] Sewu, D. D.; Boakye, P.; Woo, S. H. Adsorption of Cationic Dye by Biochar from Korean Cabbage Waste. *Bioresour. Technol.* **2017**, *224*, 206–213. https://doi.org/10.1016/j.biortech.2016.11.009

[53] Al-Shehri, H. S.; Almudaifer, E. A.; Alorabi, Q.; Alanazi, H. S.; Alkorbi, A. S.; Alharthi, F. A. Effective Adsorption of Crystal Violet from Aqueous Solutions. *Environ. Pollut. Bioavailability* **2021**, *33*(1), 214–226. https://doi.org/10.1080/26395940.2021.1960199

[54] Rajeswari, K. M.; Revanth, T.; Anirudh, A.; Prasad, B. Removal of Crystal Violet Using Water Hyacinth. *Resour.-Effic. Technol.* **2017**, *3*, 71–77. https://doi.org/10.1016/j.reffit.2017.01.009